Morphological study of early-stage lung cancer using synchrotron radiation

10 authors, including:

Some of the authors of this publication are also working on these related projects:

Transition metal chalcogenides View project

Brain cancer View project

Morphological study of early-stage lung cancer using synchrotron radiation

Ping Liu,[a] **Jianqi Sun,**[a] **Yijing Guan,**[a] **Weisheng Yue,**[b] **Lisa X. Xu,**[a]* **Yan Li,**[b] **Guilin Zhang,**[b]* **Yeukuang Hwu,**[c] **Jung Ho Je**[d] **and G. Margaritondo**[e]

[a]Key Laboratory of Systems Biomedicine, Ministry of Education, School of Life Sciences and Biotechnology, Shanghai Jiao Tong University, Shanghai 200240, People's Republic of China, [b]Shanghai Institute of Applied Physics, Chinese Academy of Sciences, Shanghai 201800, People's Republic of China, [c]Institute of Physics, Academia Sinica, Nankang, Taipei, Taiwan, [d]Department of Material Science and Engineering, Pohang University of Science and Technology, Pohang, Korea, and [e]Ecole Polytechnique Fédérale de Lausanne, CH-1015 Lausanne, Switzerland.
E-mail: lisaxu@sjtu.edu.cn, glzhang@sinap.ac.cn

In the present study the feasibility of applying synchrotron radiation to the morphological study of early-stage lung cancer has been investigated. Lewis lung cancer was implanted and grown in a nude mouse for different periods, and imaged using phase-contrast synchrotron X-rays. Morphological differences were clearly shown between the normal lung and cancerous tissues at this early stage. Irregular and tortuous angiogenesis were found in the periphery region of the developing lung cancer. Results from this study indicate that synchrotron X-rays can be used for imaging cancer development and progression with minimal invasion.

Keywords: phase-contrast X-ray imaging; lung cancer; angiogenesis.

1. Introduction

Lung cancer is one of the leading causes of death, and its incidence is increasing globally (Alberg & Samet, 2003). The five-year survival rate is approximately 14%, which has not changed over the past several decades (Kassis, 2003). Early detection is a key to the cure of lung cancer, but a difficult task to be undertaken (Deppermann, 2004; Kawabata & Ueno, 1999). Imaging techniques such as X-rays and computed tomography (CT) are often used for lung cancer detection. Conventional X-rays utilize absorption imaging, which shows the presence of details in the sample owing to different attenuation coefficients of different tissues. However, it is very difficult to discriminate cancer lesions from normal tissues because there is almost no difference in the linear attenuation coefficients of most soft tissues (Takeda et al., 2000). Phase-contrast imaging, on the other hand, using the typical edge-enhancement mechanism by refractive index (Kono, Yamasaki et al., 2001), greatly enhances the differences among soft tissues and can be used to reveal the tissue structures without using contrast agents.

The large difference in the refractive index between air and soft tissues makes the lung an ideal candidate for phase-contrast imaging (Suzuki et al., 2002; Kitchen et al., 2004). Generally, lung cancer forms some pulmonary nodules in tissue, and a different refractive index also exists between lung cancer and the rudimental normal lung tissue. These morphological differences may be clearly observed using phase-contrast imaging with synchrotron radiation X-rays.

Synchrotron radiation (SR) is characterized by its high intensity, tunable energy, polarization and small divergence. It has recently been introduced as a substitute for conventional X-rays allowing high spatial resolution up to the micrometre scale and high-speed imaging (Jung et al., 2005; Meuli et al., 2004). Phase-contrast X-ray radiography with SR has been widely applied in medical research, e.g. K-edge coronal angiography imaging (Peterzol et al., 2006), tumor angiogenesis imaging without contrast agents (Yamashita et al., 2001), lung imaging (Sera et al., 2004), cerebellar structure imaging (Momose & Fukuda, 1995), cancer lesion (Takeda et al., 1995) and so on. Mammography with SR X-rays has been carried out in clinical experiments at the SYRMEP beamline of the SR facility ELETTRA (Trieste, Italy) (Castelli et al., 2007; Arfellia et al., 2007). The combination of structural SR transmission X-rays with functional fluorescent X-rays successfully revealed the hyperthyroidism of human thyroid specimen, a fatty acid metabolic agent labelled rat's myocardium, and the first ever in vivo mouse brain structure (Takeda et al., 2001; Takeda, 2005; Wu et al., 2006). Potentially, SR X-rays could become a very powerful tool in biological and medical applications.

At present, most of the reports on phase-contrast SR X-ray imaging of tumor tissue are in vitro, except for breast cancer. In vivo phase-contrast SR X-ray imaging has been used in

normal lung of normal mice. Moreover, study of tumor angiogenesis using phase-contrast SR X-ray imaging has just begun. In this paper, phase-contrast SR X-ray imaging has been used for the first time to investigate the structural characteristics of lung cancer development in a nude mouse model. Early-stage lung cancer angiogenesis was observed in comparison with the histological analysis.

2. Materials and methods

2.1. Animal model

BALB/c nude mice (20 ± 2 g, 5 week) were bought from the Animal Center, CAS, Shanghai, China. They were fed with sterile food, acidified water with the pH value kept at 2.5–2.8, and housed in isolated cages with a 12 h light/dark cycle. Lewis lung cancer cells were cultured in medium1640 with 10% FBS (fetal bovine serum). Cells were grown in a 5% CO_2 incubator until 90% confluent and then harvested at a concentration of 1–2×10^6 cells ml^{-1} (Huang *et al.*, 1999). The window chamber was surgically placed on the dorsal skin flap of the nude mouse, and 0.1 ml lung cancer cells inoculated into the skin tissue within the window chamber. The vasculature of the tumor was clearly observed on the eleventh day after implantation. At the same time, 0.1 ml lung cancer cells were surgically transplanted into the nude mice using the percutaneous inoculation method. On the seventh day after inoculation, solitary pulmonary nodules could be observed in the nude mice. The cancer nodules were excised on the seventh, ninth and eleventh days and fixed with 10% buffered formalin. Specimens were cut into 2 mm-thick sections and imaged using phase-contrast SR X-rays. Correlative tissue samples were further cut into 5 μm-thick slices and stained with hematoxylin and eosin. Histological study was performed using a $100\times$ oil objective and images were recorded under the trans-illumination light.

For the *in vivo* experiment, BALB/c nude mice (16–21 g, 5 week) were bought from the Animal Center, Japan. On the 14th day after the implantation of the Lewis lung cells, the mice were imaged live.

2.2. Phase-contrast imaging with SR X-rays

Lung cancer imaging was performed at the International Consortium of Phase Contrast Imaging and Radiology (7B2) beamline of Pohang Light Source (PLS) in Korea. The PLS is designed to provide SR with continuous wavelengths down to 10 nm, at 2.5 GeV. The experimental set-up is similar to that presented by Baik *et al.* (2004) and Hwu *et al.* (2004), and is schematically shown in Fig. 1. The detection system consists of a thin (100 μm) CdWO$_4$ cleaved single-crystal scintillator and a CCD camera. In our experiment, polychromatic synchrotron X-rays were used with an energy range of 4–14 keV.

A key parameter in phase-contrast radiology is the distance between the specimen and the detector. At 20–40 cm from the detector, other types of effects such as Fresnel diffraction fringes can be washed out and the refraction effect can be optimized (Kitchen *et al.*, 2004). The experimental parameters

for the phase-contrast imaging of lung cancer with SR X-rays were set as follows: an exposure time of 50 ms, magnification of $20\times$, and specimen–detector distance of 20 cm. For comparison, absorption images were also recorded at the same time with a specimen–detector distance of 2 cm.
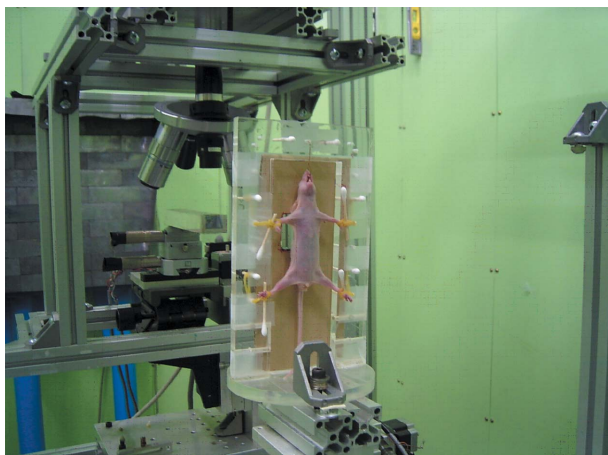
2.3. Image reconstruction

The samples were mounted on a translation/rotation stage that was controlled by a step motor allowing precise positioning. For biological samples with intrinsically limited X-ray phase contrast, a single image (typically 1600×1200 pixels, horizontal field of view 540 μm) could be recorded within 50 ms. Four images were recorded at each position and averaged. The final image was obtained by subtracting the background acquired at the same height but without a specimen. The samples were usually 2–3 mm in both length and width, and arrays of images should be projected accordingly and patched automatically using *Image Pro Plus* (Yue *et al.*, 2007). Subsequently, the areas of interest, usually the edge of the cancer with plenty of angiogenesis, were chosen. The stage should be aligned horizontally to include the areas of interest in the image field. Serial images were recorded automatically every $0.5°$ by the step motor through the standard filter-back projection algorithm process. The images were input into the *Amira* software (Hwu *et al.*, 2004) for three-dimensional display. The corresponding radiation did not produce any detectable damage to tissue visually.

2.4. Observation of lung cancer in live mice

The anaesthetized mouse [ketamine-xylazine 5 ul g^{-1}, ip (intraperitoneal injection)] was mounted on a customized
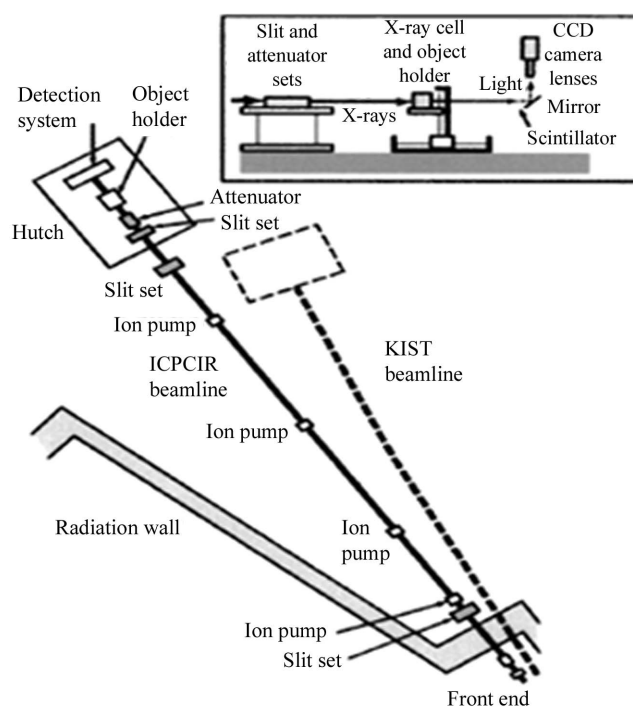
Figure 1
Overall scheme of the beamline and (inset) of the radiography system (Baik *et al.*, 2004).

Figure 2
Experimental set-up for imaging live mice.

Figure 3
Lewis lung cancer angiogenesis viewed with a 10× objective (*a*) on the ninth day and (*b*) on the eleventh day. Scale bar: 200 µm.

plastic shaft as shown in Fig. 2. The window size on the shaft was about 3 cm × 3 cm, through which the X-rays passed. The mouse chest was positioned at the window. A single image (typically 533 × 400 pixels, horizontal field of view 2.7 mm) could be recorded within 2 ms. In order to obtain the images without the influence of background, three images were recorded at each position and then averaged, and the background acquired at the same height was subtracted from the averaged image. Given the size of the chest area, more than 10 × 10 arrays of images were acquired. These images were then patched together to obtain the whole image of the chest.

Since the exposure time was within 1 min in total, the corresponding radiation dose did not produce any detectable damage over the whole process. Image processing was then performed to distinguish the cancer from the normal tissue.
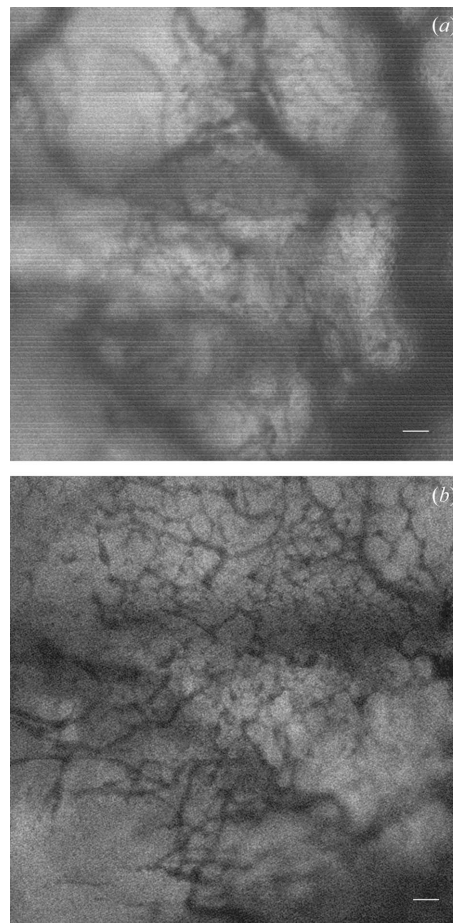
3. Results

3.1. Characteristic of tumor angiogenesis

Fig. 3 illustrates the Lewis lung cancer angiogenesis process using white-light images recorded on the ninth and eleventh day after the lung cancer was implanted in the dorsal skinfold window. There was no change in the vessel branching pattern observed in the implantation region and the surrounding host in the first several days. On the ninth day, irregularly formed, tortuous, irregular and early tumor angiogenesis was observed in the cancer periphery region. More abundant angiogenic sprouts appeared on the eleventh day and irregular dilated, tortuous larger vessels were found inside the tumor.

3.2. Morphological observation of early-stage lung cancer samples with SR X-rays

Figs. 4(*a*)–4(*c*) show the phase-contrast and absorption images recorded using SR X-rays. Normal structures of venules and air sacs are clearly illustrated in Fig. 4(*a*), similar to that reported by Kono, Ohbayashi *et al.* (2001). Images of the formalin-fixed lung cancer tissues dissected on different days after the implantation were recorded. On the eleventh day, significant differences could be found in structures between the cancerous and normal lung tissues. For comparison, the absorption and phase-contrast images of the Lewis lung cancer dissected on the eleventh day after the implantation are shown in Figs. 4(*b*) and 4(*c*), respectively. In Fig. 4(*b*) the boundary between cancerous and normal tissues is distinguishable. Tumor cells are closely packed to form dense and smooth cancerous tissue, and irregularly formed and tortuous early cancer angiogenesis can be observed in the periphery region. Fig. 4(*c*) shows the lower half part of the nodule presented in Fig. 4(*b*) taken at the same magnification. In comparison, the phase-contrast image more clearly reveals a distinguishable boundary between cancerous and normal tissues, as well as air sacs, mildly thickened alveolar walls and tortuous angiogenesis, than that in the absorption image. These structures are similar to those observed through morphological study as shown in Fig. 3.

A corresponding histopathological study of the lung cancer specimens (eleventh day) was performed and the detailed structures observed using SR X-rays were confirmed. In Fig. 5(*a*), terminal bronchiole and air sacs are seen clearly. On the other hand, while lung cancer cells have completely
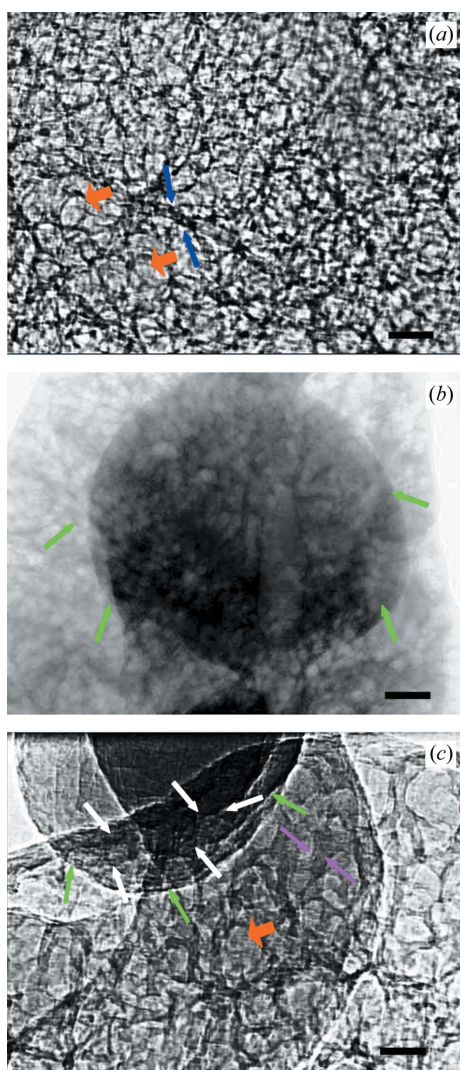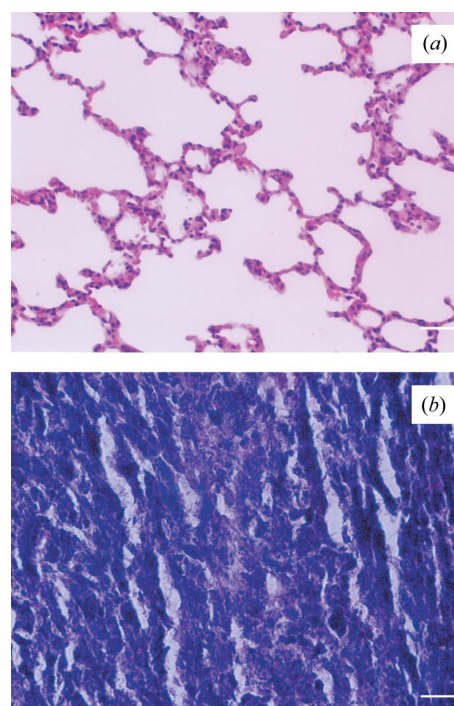
Figure 4
SR X-ray imaging of lung cancer samples obtained on the eleventh day after implantation. (*a*) Phase-contrast SR image of normal lung tissue: venules (blue arrows) and air sacs (red arrows). (*b*) Absorption image of lung cancer: tumor boundary (green arrows). (*c*) Phase-contrast SR image of lung cancer: tortuous early cancer angiogenesis (white arrows) and the periphery region of the cancerous tissue (green arrows); air sacs (red arrow) and thickened alveolar walls (pink arrows). Scale bar: 40 µm.

Figure 5
Histological sections of the Lewis lung cancer. (*a*) Normal lung tissue. (*b*) Lung cancer tissue (eleventh day). Scale bar: 10 µm.

occupied the terminal bronchiole and air sacs, normal lung structures can no longer be seen in Fig. 5(*b*).

3.3. Three-dimensional image reconstruction

Fig. 6 shows the patched image and partial tomographic reconstruction of the normal lung specimen. An injector tip, which is visible in the middle of Fig. 6(*a*), was used to fix the sample to the holder. As identified by the arrow, alveolus can be easily found on the edge of the specimen, while in the middle of the image it is somewhat blurred because of the thickness. The trachea or the bronchia can be seen in the specimen. The white box indicates the area of interest, which was tomographically reconstructed using the conventional filter-back projection algorithm. Fig. 6(*b*) shows one layer of

the tomographic images indicated by the red line in Fig. 6(*a*). The reconstruction was based on 180 projections within 2 min. It clearly reveals the alveolus wall. The quality of the reconstruction was compromised owing to the slight movement of the sample during the measurement and possible 'local tomography' effects mentioned by Takeda *et al.* (2006) and Ando *et al.* (2005).

At the same time, lung cancer sample imaging was also performed. Fig. 7(*a*) shows the lung cancer image taken on the eleventh day after the implantation. The area of interest indicated in the white box was reconstructed using a similar algorithm as mentioned above. Fig. 7(*b*) presents one of the tomographic images outlined by the red line in Fig. 7(*a*). Although the entire region is rather uniform without much observed structure, the thickened wall of the alveolus is clearly shown.

3.4. SR X-ray imaging *in vivo*

Lung tissues in live mice were also imaged using SR X-rays. Fig. 8 shows the projection image of the chest area with Lewis lung cancer implanted. The whole chest image was obtained from patched serial images. The smaller exposure time was necessary to avoid the motion caused by the heart beating, and polychromatic synchrotron X-rays were used in the imaging. The patched image seemed well tiled because the mouse was fastened and the influence of slight breathing could be omitted in the short period of 2 ms for each imaging.

The anatomic structures of the chest including heart, bones and thorax can be distinguished clearly in the image. On the left-hand side, the lung cancer was identified as higher density
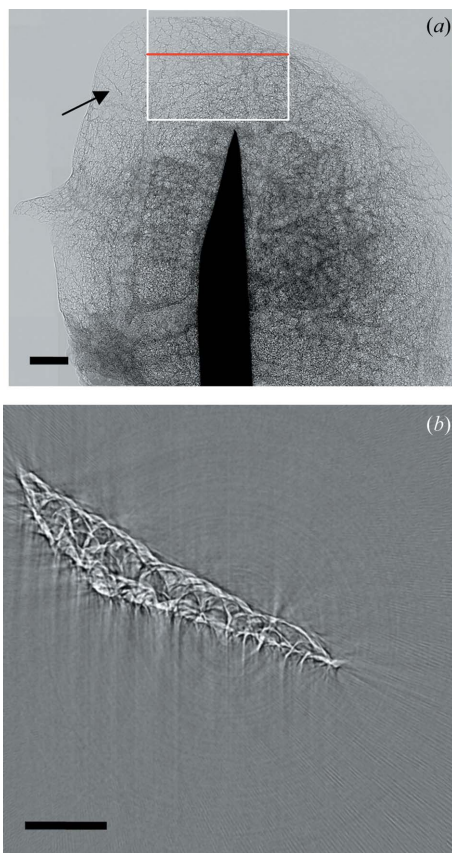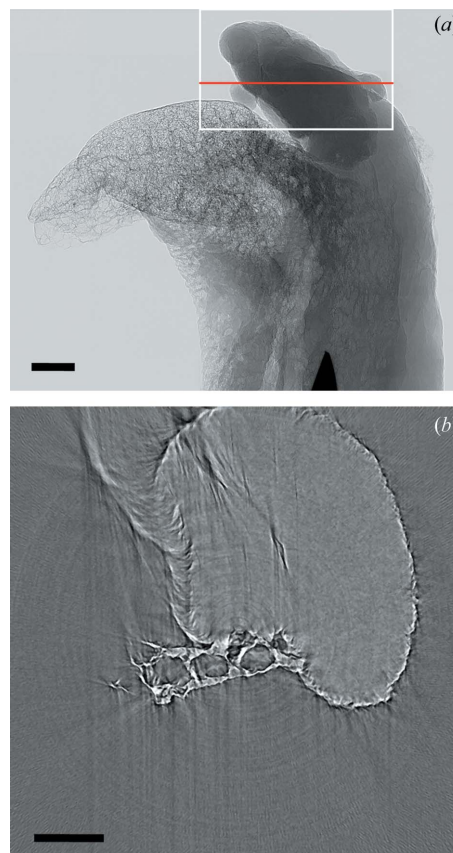
Figure 6
Images of normal lung specimen. (*a*) Patched phase-contrast micrograph of the whole specimen; an injector's tip was used to fix the specimen to the holder. The white box indicates the area of interest. Scale bar: 200 μm. (*b*) Tomographic reconstruction of part of the same specimen.

Figure 7
Images of lung cancer specimen on the eleventh day. (*a*) Patched phase-contrast micrograph of the whole specimen; an injector's tip was used to fix the specimen to the holder. The white box indicates the area of interest. Scale bar: 200 μm. (*b*) Tomographic reconstruction of part of the same specimen.

compared with that of the normal tissue. The black part in the middle of the image on the right was caused by a shutter-opening error that occurred during imaging.

The single imaging exposure time *in vivo* was only 2 ms per exposure. In this period the shutter was opened from the bottom left to the top right, resulting in more exposure to the lower left-hand part which appeared brighter than the upper part. This is the cause of the stripes in the image. As the shutter movement was proportional to time, the grey-level change could be regarded as linear. For correction, we first divided each row of the image by a background taken accordingly without objects in the object holder. This smooths the images and removes noise caused by the camera. As the stripes are regarded similarly to flat-fielding in optical imaging, a gradient with a gradually changing grey-level was applied for division correction. The black part caused by the shutter error was also corrected by flat-fielding. The result is shown in Fig. 9, and the lung cancer is much clearer as indicated in the red rectangular box.

In order to automatically detect the lung cancer tissue using grey-scale quantification, the image information of the ribs should be removed. The image was firstly filtered by the Roberts operator to enhance the fine edges. Then the rib signals were almost removed, but the image became blurred.

Therefore, a gauss filter was also used for signal enhancement. Combining these two methods, the final image is shown in Fig. 10. The brighter parts of the image are the thorax. It may have introduced some noise, but it does enhance the unusual shadow (indicated by the red line) appearing at the lower left-hand part of the thorax, which is a cancer tumor.

We used plot profile analysis (*Image Pro Plus*) to outline the cancer tissue appearing in Fig. 10. The average grey-scale level of lung cancer tissue is about 35% of the average grey-scale level of the left half lung tissue. This provides quantitative evidence that the lung cancer tissue has a higher density than its surrounding thorax, and it appears darker with a lower grey-scale level.

4. Discussion

X-ray chest imaging, CT, magnetic resonance imaging (MRI), isotopes, bronchoscopy *etc.* are commonly used for lung cancer diagnosis. CT is a potential tool for revealing small cancers presumably at stage I, but as yet only in theory (Henschke *et al.*, 1999; Marcus *et al.*, 2000). Presently, MRI seems an ideal diagnostic method for determining the cancer character, configuration and positioning for small sizes;
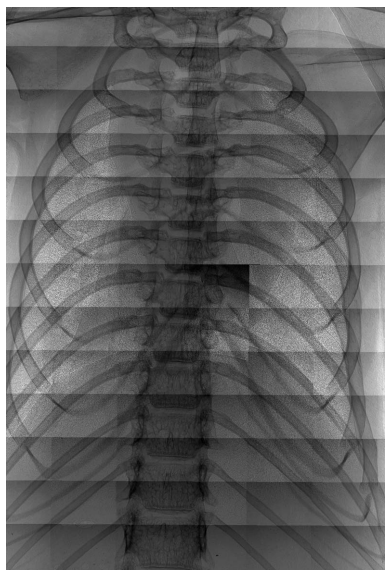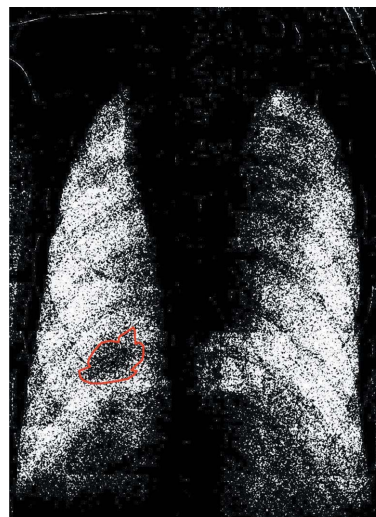
Figure 8
Chest area of a live mouse with implanted lung cancer viewed using SR X-rays.
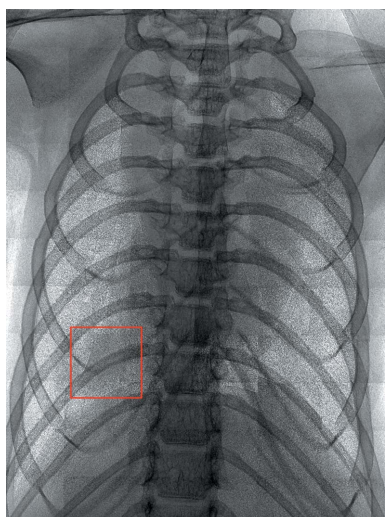
Figure 9
Enhanced image after flat-field division.

Figure 10
Image with the ribs removed. The lung cancer tissue is outlined in red.

however, it usually requires contrast agents (Xu *et al.*, 2000). Despite the rapid advancement in biomedical imaging technology, there has not been any significant reduction in cancer mortality in the last two decades (Fontana *et al.*, 1984; Frost *et al.*, 1984; Melamed *et al.*, 1984; Kubik & Polak, 1986). Neither CT nor MRI can be used to clearly detect the detailed structures on the micrometre scale for early diagnosis of cancers (Kubik & Polak, 1986; Furman-Haran *et al.*, 1998; Laib & Rüegsegger, 1999).

The aim of this study was to investigate the radiological and pathological characteristics of lung cancer at an early stage using SR X-ray phase-contrast imaging. The high flux and brightness of the SR beam provides an ideal X-ray source for many applications in medical science, such as X-ray microscopy of biological structures and applications of *in vivo* imaging. Because refraction imaging with SR emphasizes the edge effect of the structures contained in an object, it can be used to observe very fine structures of biological tissues at the micrometre level. In the present study, the SR images have depicted the structures of the normal and cancerous lung tissues for sizes ~2 mm thick. Compared with the conventional absorption image, the phase-contrast image using SR X-rays showed much better image contrast. Fine internal structures of the lung cancer tissue were visualized through edge contrast enhancement. In thick slices there are numerous pulmonary structures overlapping each other. The overlapped structures, including cancer, normal tissue and newly developed blood vessels, were mostly revealed by SR imaging. The corresponding pathological studies have confirmed the findings obtained by SR imaging. The phase-contrast image using SR showed cancer cells and vascular invasion in the periphery region. Angiogenesis is a complex process involving cancer growth and cancer metastasis *etc*. It would be essential for early cancer diagnosis if newly developed vessels could be detected accurately using SR imaging. The tomographic reconstructed images in this paper are our first step; more work should be done on this aspect according to the literature (Majumdar *et al.*, 1998; Sera *et al.*, 2005). In the thorax, because bone and other soft tissues overlap with the lung tissue in most optical images, subtraction and stereoscopic imaging and longitudinal or axial computed tomography with SR should be performed *in vivo*. The preliminary results presented in this paper have shown the feasibility of applying SR X-ray imaging for early lung cancer investigation.

research papers

References

Alberg, A. J. & Samet, J. M. (2003). *Chest*, **123**, S21–S49.
Ando, M. *et al.* (2005). *Nucl. Instrum. Methods Phys. Res. A*, **548**, 1–16.
Arfellia, F. *et al.* (2007). *Ninth International Conference on Synchrotron Radiation Instrumentation, AIP Conference Proceedings 879*, pp. 1895–1898. Melville: American Institute of Physics.
Baik, S., Kim, H. S., Jeong, M. H., Lee, C. S., Je, J. H., Hwu, Y. & Margaritondo, G. (2004). *Rev. Sci. Instrum.* **75**, 4355–4358.
Castelli, E. *et al.* (2007). *Nucl. Instrum. Methods Phys. Res. A*, **572**, 237–240.
Deppermann, K. M. (2004). *Lung Cancer*, **45**, S39–S42.
Fontana, R. S., Sanderson, D. R., Taylor, W. F., Woolner, L. B., Miller, W. E., Muhm, J. R. & Uhlenhopp, M. A. (1984). *Am. Rev. Respir. Dis.* **130**, 561–565.
Frost, J. K., Ball, W. C. Jr, Levin, M. L., Tockman, M. S., Baker, R. R., Carter, D., Eggleston, J. C., Erozan, Y. S., Gupta, P. K., Khouri, N. F., Marsh, B. R. & Stitik, F. P. (1984). *Am. Rev. Respir. Dis.* **130**, 549–554.
Furman-Haran, E., Margalit, R., Grobgeld, D. & Degani, H. (1998). *J. Magn. Res. Imag.* **8**, 634–641.
Henschke, C. I., McCauley, D. I., Yankelevitz, D. F., Naidich, D. P., McGuinness, G., Miettinen, O. S., Libby, D. M., Pasmantier, M. W., Koizumi, J., Altorki, N. K. & Smith, J. P. (1999). *Lancet*, **354**, 99–105.
Huang, Q., Shan, S., Braun, R. D., Lanzen, J., Anyarambhatla, G., Kong, G., Borelli, M., Corry, P., Dewhirst, M. W. & Li, C.-Y. (1999). *Nat. Biotechnol.* **17**, 1033–1035.
Hwu, Y., Tsai, W. L., Je, J. H., Seol, S. K., Kim, B., Groso, A., Margaritondo, G., Lee, K. H. & Seong, J. K. (2004). *Phys. Med. Biol.* **49**, 501–508.
Jung, H., Kim, H.-J., Kim, E.-K., Hong, J.-O., Je, J. H., Hwu, Y., Tsai, W.-L., Magaritondo, G. & Yoo, H.-S. (2005). *Yonsei Med. J.* **46**, 95–103.
Kassis, A. I. (2003). *Acad. Radiol.* **10**, 1078–1079.
Kawabata, H. & Ueno, T. (1999). *Lancet*, **354**, 1206.
Kitchen, M. J., Paganin, D., Lewis, R. A., Yagi, N., Uesugi, K. & Mudie, S. T. (2004). *Phys. Med. Biol.* **49**, 4335–4348.

Kono, M., Ohbayashi, C., Yamasaki, K., Ohno, Y., Adachi, S., Sugimura, K. & Suzuki, Y. (2001). *Acad Radiol.* **8**, 898–902.
Kono, M., Yamasaki, K., Ohno, Y., Adachi, S., Sugimura, K. & Suzuki, Y. (2001). *Acad. Radiol.* **8**, 898–902.
Kubik, A. & Polak, J. (1986). *Cancer*, **57**, 2427–2437.
Laib, A. & Rüegsegger, P. (1999). *Bone*, **24**, 35–39.
Majumdar, S., Kothari, M., Augat, P., Newitt, D. C., Link, T. M., Lin, J. C., Lang, T., Lu, Y. & Genant, H. K. (1998). *Bone*, **22**, 445–454.
Marcus, P. M., Bergstralh, E. J., Fagerstrom, R. M., Williams, D. E., Fontana, R., Taylor, W. F. & Prorok, P. C. (2000). *J. Natl. Cancer Inst.* **92**, 1308–1316.
Melamed, M. R., Flehinger, B. J., Zaman, M. B., Heelan, R. T., Perchick, W. A. & Martini, N. (1984). *Chest*, **86**, 44–53.
Meuli, R., Hwu, Y., Je, J. H. & Margaritondo, G. (2004). *Eur. Radiol.* **14**, 1550–1560.
Momose, A. & Fukuda, J. (1995). *Med. Phys.* **22**, 375–379.
Peterzol, A. *et al.* (2006). *Radiat. Protect. Dosim.* doi:10.1093/rpd/nci710.
Sera, T., Uesugi, K. & Yagi, N. (2005). *Med. Phys.* **32**, 2787–2792.
Sera, T., Yagi, N. & Uesugi, K. (2004). *Proceedings of the 26th Annual International Conference of the IEEE EMBS*, San Francisco, USA, pp. 1294–1297. Piscataway: IEEE Press.
Suzuki, Y., Yagi, N. & Uesugi, K. (2002). *J. Synchrotron Rad.* **9**, 160–165.
Takeda, T. (2005). *Nucl. Instrum. Methods Phys. Res. A*, **548**, 38–46.
Takeda, T., Momose, A., Hirano, K., Haraoka, S., Watanabe, T. & Itai, Y. (2000). *Radiology*, **214**, 298–301.
Takeda, T., Momose, A., Itai, Y., Jin, W. & Hirano, K. (1995). *Acad. Radiol.* **2**, 799–803.
Takeda, T., Wu, J., Thet-Thet Lwin, Yoneyama, A., Hirai, Y., Hyodo, K., Sunaguchi, N., Yuasa, T., Minami, M., Kose, K. & Akatsuka, T. (2006). *Proc. SPIE*, **6318**, 63180W.
Takeda, T., Yu, Q., Yashiro, T., Zeniya, T., Wu, J., Hasegawa, Y., Thet-Thet Lwin, Hyodo, K., Yuasa, T., Dilmanian, F. A., Akatsuka, T. & Itai, Y. (2001). *Nucl. Instrum. Methods Phys. Res. A*, **467–468**, 1318–1321.
Wu, J., Takeda, T., Thet-Thet Lwin, Sunaguchi, N., Fukami, T., Yuasa, T., Minami, M. & Akatsuka, T. (2006). *Proc. SPIE*, **6318**, 631828.
Xu, J., Yu, Z. & Jiang, W. (2000). *Radiol. Prac.* **15**, 187–189.
Yamashita, T. *et al.* (2001). *Invest. Radiol.* **36**, 713–720.
Yue, W. S., Zhang, G., Liu, P., Sun, J., Hwu, Y., Je, J. H., Tan, M. & Li, Y. (2007). *Nucl. Instrum. Methods Phys. Res. B*, **262**, 304–312.